Nationaal Lucht- en Ruimtevaartlaboratorium
National Aerospace Laboratory NLR

NLR-TP-2002-223

On the use of characteristics in computational aeroacoustics

J.B.H.M. Schulten

Nationaal Lucht- en Ruimtevaartlaboratorium
National Aerospace Laboratory NLR

NLR-TP-2002-223

On the use of characteristics in computational aeroacoustics

J.B.H.M. Schulten

The content of this paper have been published as AIAA paper 2002-2584 in the Proceedings of the 8th AIAA/CEAS Aeroacoustics Conference, Breckenridge, Colorado, USA, 17-19 June 2002.

Customer:	National Aerospace Laboratory NLR
Working Plan number:	A.1.C.2
Owner:	National Aerospace Laboratory NLR
Division:	Fluid Dynamics
Distribution:	Unlimited
Classification title:	Unclassified
	April 2002

Contents

(12 pages in total)

ON THE USE OF CHARACTERISTICS IN COMPUTATIONAL AEROACOUSTICS

Johan B.H.M. Schulten*
National Aerospace Laboratory NLR, 8300 AD Emmeloord, The Netherlands

Abstract

Although most CAA schemes for the numerical simulation of sound propagation in flows offer significant superiority compared to standard CFD methods, their performance still crucially depends on a sufficient number of grid points per wavelength. For a given grid density only waves of a length scale beyond a certain limit can be resolved accurately. Even for harmonic sound the shortest wavelengths are not always known in advance of solving the problem and accuracy has to be established by systematic grid refinement. For non-smooth wave shapes most numerical schemes suffer from spurious dispersion. This behavior occurs even under the ideal conditions of small amplitude, plane sound waves in a uniform background fluid. The present paper outlines an alternative method that is able to model the propagation under these conditions exactly, irrespective of the number of points per wavelength or wave shape. The method is based on the concept of characteristics, i.e. the propagation directions of the pressure waves. Unlike fixed grid methods, the coordinates of the data points are found by tracking the characteristics during the solution process. The implementation of non-reflecting boundary conditions is exceptionally straightforward. The method is illustrated by two- and three-dimensional benchmark cases.

Nomenclature

c	= speed of sound
i	= unit vector
M	= vector mean flow Mach number
M	= scalar mean flow Mach number
p	= pressure
r	= radial coordinate
t	= time
u	= axial velocity
v	= velocity
W	= reference system velocity
x	= absolute position vector
x,ξ	= axial coordinate
ρ	= mass density

Subscripts

0	= mean value
a	= acoustic
h	= hydrodynamic
r	= normal to wave front
q, s	= parallel to wave front

Superscript

$*$	= dimensional quantity

Introduction

Traditionally, the theoretical modeling of sound propagation is based on analytical methods. Only in the last decade computers have become sufficiently powerful to consider a fully numerical approach of real life problems. Attempts to use standard second order accurate CFD (Computational Fluid Dynamics) numerical schemes for sound propagation almost invariably yield disappointing results. Unless a large number of grid points (typically 50 or more) per wavelength is adopted, the simulations suffer from severe spurious dissipation and dispersion.

This shortcoming of CFD methods promoted the rise of Computational AeroAcoustics (CAA) in the nineties of the last century. This discipline studies the efficient and accurate numerical simulation of sound propagation and generation in flows.

One of the most successful CAA methods that emerged is Tam & Webb's DRP (Dispersion Relation Preserving) scheme[1]. It is a high order explicit finite difference method that can be easily applied to a variety of aeroacoustic problems. The DRP-scheme yields accurate results for only 8 grid points per wavelength. Compared with some 50 points required for common CFD methods this implies a reduction factor of 6 in 1D problems and a spectacular factor of more than 200 in 3D problems. Reviews on the state of the art in CAA can be found in references[2,3,4].

*Research Fellow, Aeroacoustics Department P.O.Box 153, E-mail: schulten@nlr.nl, Senior Member AIAA.

Generally speaking, CAA numerical schemes are dissipation-free, high order schemes, optimized for minimum numerical dispersion. Although these methods require much less points per wavelength to achieve a certain level of accuracy than the standard CFD methods, they still have their limits. Sometimes the wave shapes to be studied are not smooth and contain higher harmonics, for which the grid density is still too coarse.

The present paper addresses the possibilities of using characteristics (propagation directions in space-time) for numerical modeling of sound wave propagation. Unlike the CAA-methods mentioned above, the method of characteristics does not use a fixed grid. Instead, the propagation vector of the wave fronts is tracked in space-time for all initial data points. This approach is similar to the concepts of wave fronts and rays that were developed by Huygens and Fermat[5] in the 17th century. However, in the present study we will not need the high frequency assumption of ray acoustics.

The method also follows the basic ideas of Riemann's theory[6] to solve the general nonlinear problem of gas dynamics in one space dimension. Along the characteristics the so-called Riemann invariants, or characteristic variables, are constant. The extension to multiple space dimensions is non-trivial, since the characteristic variables are no longer constant along the characteristic (hyper) surfaces. It will be shown that their variation readily follows from the flow equations.

After some simple examples to introduce the method, the general formulation in two and three dimensions will be derived. In this paper only linear problems with a uniform background flow will be addressed. In the numerical simulation a standard 4th order Runge-Kutta scheme[7] is used for integration along the characteristic direction. An important advantage of the present method is that the implementation of non-reflective boundary conditions, as well as outflow conditions is almost trivial, also in higher dimensions. The method will be illustrated by two- and three-dimensional benchmark cases.

Simple 1D theory and examples

Let us consider a perturbed homentropic fluid without mean flow in one space dimension. Ignoring thermal conductivity and viscosity, the flow equations reduce to the Euler equations. Using the mean fluid density and speed of sound and some arbitrary length (or time step) to make the Euler equations nondimensional, we obtain:

$$\frac{\partial p}{\partial t} + \frac{\partial u}{\partial x} = 0 \qquad (1)$$

$$\frac{\partial u}{\partial t} + \frac{\partial p}{\partial x} = 0 \qquad (2)$$

As can be readily verified, this set of equations has the following analytical solution

$$p(x,t) = p_R(x - t, 0) + p_L(x + t, 0) \qquad (3)$$

and

$$u(x,t) = p_R(x - t, 0) - p_L(x + t, 0) \qquad (4)$$

where $p_R(x,0)$ and $p_L(x,0)$ are the initial values of the right running and left running pressure waves.

As first step in the method of characteristics Eq.(1) and Eq.(2) are summed, which yields:

$$\frac{\partial(p + u)}{\partial t} + \frac{\partial(p + u)}{\partial x} = 0 \qquad (5)$$

Similarly, the subtraction of Eq.(1) and Eq.(2) yields:

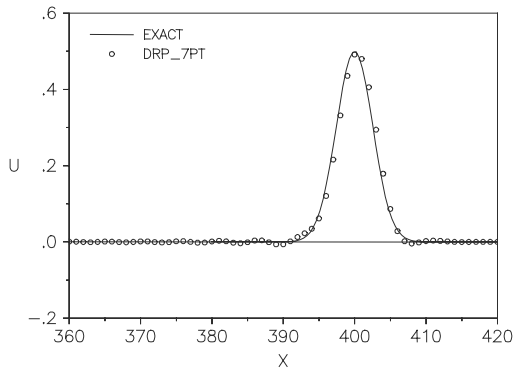

Fig.1 Gaussian pulse $t = 400$, DRP scheme

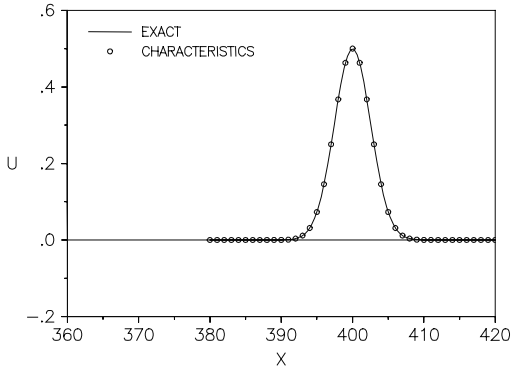

Fig.2 Gaussian pulse $t = 400$, present method

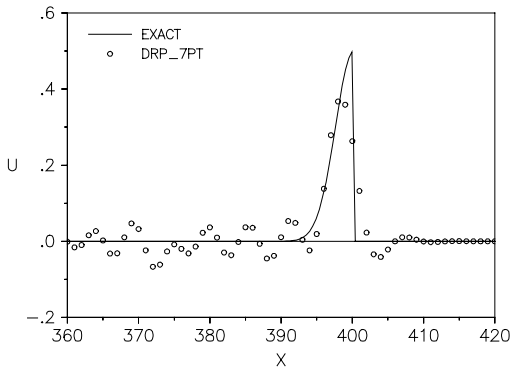

Fig.3 Half a Gaussian pulse t = 400, DRP scheme

$$\frac{\partial(p-u)}{\partial t} - \frac{\partial(p-u)}{\partial x} = 0 \qquad (6)$$

Now, from Eq.(5) it is obvious that the increase of quantity (p+u) in time dt is compensated by an equal decrease in space dx . In other words the quantity is constant along lines dx/dt = 1, which are called the forward characteristics because they advance with time.
As a result, along the forward characteristics:

$$\left[\frac{d(p+u)}{dt}\right]_{dx/dt=1} = 0 \qquad (7)$$

i.e., quantity (p+u) propagates forward with (non-dimensional) unit velocity. It can be shown that this quantity is the nondimensional, linear perturbation equivalent of the forward Riemann invariant[6]:

$$u^* + \tfrac{2}{\gamma-1}c^* = \left[M + u + \tfrac{2}{\gamma-1} + p\right]c_0^* \qquad (8)$$

where γ is the ratio of specific heats of the medium. Quite similarly, we have along the backward characteristics:

$$\left[\frac{d(p-u)}{dt}\right]_{dx/dt=-1} = 0 \qquad (9)$$

Let us illustrate this result by means of the first Cat.1 benchmark problem of the first CAA Workshop[8] : the propagation of a forward propagating Gaussian pulse with the exact solution:

$$u(x,t) = 0.5\exp\left[-(\ln 2)\left(\frac{x-t}{3}\right)^2\right] \qquad (10)$$

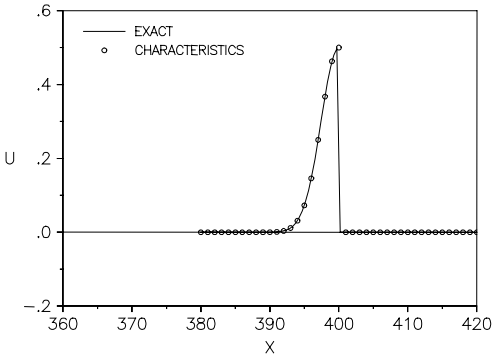

Fig.4 Half a Gaussian pulse t = 400 , present method

The problem is given as an initial value problem at t = 0 with p(x,0) = u(x,0). As follows from Eq.(1) or Eq.(2), then there is only a right running wave. In Fig.1 the result of Tam & Webb's scheme with unit spacing and a time step Δt = 0.2 is shown for t = 400. The time step is scaled on unit spacing of the data points and the speed of sound. Therefore, Δt is identical to the CFL number in this case. Obviously, the result is quite good with only some weak dispersion.
The result of solving Eq.(7) for the advancing characteristic variable, given in Fig.2, is independent of the time step and can be obtained from a single time step of 400. Indeed, this problem is so simple that the numerical solution by Runge-Kutta integration of Eq.(7) seems to be pointless. Apart from being discrete it perfectly mimics the analytical solution given by Eqs.(3) and (4). Also, it clearly demonstrates the difference with fixed grid methods since the original data points are shifted to the right over a distance of 400. As may be expected, the result is accurate to machine precision.
As shown in Fig.3 things dramatically change for the DRP scheme if a discontinuous waveform is taken. It is clear that the DRP scheme is unfit to handle the halved Gaussian pulse properly. In fact the large content of short waves in this shape cannot be resolved with the present grid spacing. In contrast to this, the characteristics method simulates the propagation of half a Gaussian pulse equally well as the complete pulse, as demonstrated in Fig. 4. The method does not try to approximate time or space derivatives of the wave, but directly uses the characteristic directions to propagate the signal, irrespective of its shape. Our goal will be to preserve this outstanding quality of the characteristics method in higher dimensions and for more general flow conditions. A modeling is sought that will automatically yield the accuracy observed in this section, at least when the wave

fronts tend to become planar and the background uniform.

Extension to multi-dimensions

In Arbitrary Lagrangian-Eulerian (ALE) formulation[9] the equations for small perturbations of an inviscid compressible flow with a uniform background read as follows.

Continuity:

$$\frac{\partial \rho}{\partial t} + (M - W)\bullet\nabla\rho + \nabla\bullet v = 0 \qquad (11)$$

Momentum:

$$\frac{\partial v}{\partial t} + (M - W)\bullet\nabla v + \nabla p = 0 \qquad (12)$$

Energy:

$$\frac{\partial p}{\partial t} + (M - W)\bullet\nabla p + \nabla\bullet v = 0 \qquad (13)$$

where W is the reference system velocity and M the vector background flow Mach number. The variables are made dimensionless in the same way as in the previous section.

Obviously, for W = 0 the Euler equations are obtained, while for W = M the Lagrangian flow description is recovered. It will prove useful to make use of both flow descriptions.

Note that the presence of an energy equation implies that we do no longer require a homentropic flow. In the latter case the energy equation becomes identical to the continuity equation. As a result, the system of equations will, besides acoustic waves, also describe entropy perturbations, which are convected with the mean flow.

Formally, we have as many scalar momentum equations (12) as there are spatial dimensions. Now consider for a moment a system of plane waves in three dimensions. Of course, physically this is completely equivalent to the situation of the 1D waves in the previous section. A coordinate rotation such that the x-axis becomes normal to the wave fronts, i.e. in the direction of ∇p, is sufficient to make this perfectly clear.

However, unlike the one-dimensional problem, the flow equations Eqs.(11) through (13) for the multi-dimensional problem admit the existence of nontrivial zero-pressure velocity fields v_h, corresponding to vorticity perturbations. For a vanishing pressure perturbation Eqs.(12) and (13) reduce to

$$\nabla\bullet v_h = 0 \qquad (14)$$

and

$$\frac{\partial v_h}{\partial t} + (M - W)\bullet\nabla v_h = 0 \qquad (15)$$

Clearly, any velocity field satisfying Eqs. (14) and (15) can always be added to the complete system given by Eqs.(11) through (13). Eq.(14) expresses the incompressibility of these velocity fields which are therefore also called “hydrodynamic”. The purely convective character of this hydrodynamic velocity is stated by Eq.(15). In general the amplitude of the hydrodynamic field has to be set by the boundary (inflow) conditions or the initial values.

Usually, we have a non-zero pressure gradient and then we can introduce a local, coordinate system (r,q,s):

$$i_r = \frac{\nabla p}{|\nabla p|}, \qquad i_r\bullet i_q = 0, \quad i_r\bullet i_s = 0, \quad i_s\bullet i_q = 0 \qquad (16)$$

Now let us denote the “acoustic velocity” coupled with pressure perturbation by v_a. It can be readily shown that v_a must be irrotational.

Substitution of $v = v_a + v_h$ in the momentum equation Eq. (12) reveals that $v_a = v_a i_r$. Then, in the Lagrangian description (W = M), normal to the wave front the momentum equation Eq.(12) reduces to the <u>scalar</u> equation:

$$\frac{\partial v_a}{\partial t} + \frac{\partial p}{\partial r} = 0 \qquad (17)$$

The divergence of the acoustic velocity becomes:

$$\nabla\bullet v_a = \frac{\partial v_a}{\partial r} + v_a\nabla\bullet i_r \qquad (18)$$

Now, Eq.(13) + Eq.(17) yields:

$$\frac{\partial(p + v_a)}{\partial t} + \frac{\partial(p + v_a)}{\partial r} = -v_a\nabla\bullet i_r \qquad (19)$$

and similarly Eq.(13) – Eq.(17) yields:

$$\frac{\partial(p - v_a)}{\partial t} - \frac{\partial(p - v_a)}{\partial r} = -v_a\nabla\bullet i_r \qquad (20)$$

As a result we have along the advancing characteristic:

$$\left[\frac{d(p + v_a)}{dt}\right]_{dx/dt = M + i_r} = -v_a\nabla\bullet i_r \qquad (21)$$

and along the receding characteristic:

$$\left[\frac{d(p - v_a)}{dt}\right]_{dx/dt = M - i_r} = -v_a \nabla \bullet i_r \qquad (22)$$

Along the convective characteristic (dx/dt = M) Eq.(13) – Eq.(11) yields:

$$\left[\frac{d(p - \rho)}{dt}\right]_{dx/dt = M} = 0 \qquad (23)$$

and Eq. (15) :

$$\left[\frac{dv_h}{dt}\right]_{dx/dt = M} = 0 \qquad (24)$$

Note that the characteristic variables in Eqs. (23) and (24) are invariants (also in multi-dimensions!). Just like the original Eqs.(11) through (13) for the five primitive variables, Eqs.(21) through (24) form a system of six scalar equations for six characteristic variables. However, the three components of v_h are not mutually independent because they have always to satisfy the incompressibility condition of Eq.(14).

Figure 5 gives a picture of the three types of characteristics in an Eulerian r,t-plane. Note that the skewness of the system depends on the r-component of the background flow velocity vector. In the Lagrangian frame the acoustic characteristics become symmetric about the convective characteristics which then are vertical. Note that primitive variables can only be evaluated at the intersection points of three characteristics. Hence, time step and spatial step (in r) are necessarily equal. Since the background flow vector in general does not point in the direction normal to the wave fronts this triple intersection only occurs in the Lagrangian frame.

In the degenerate case of a vanishing pressure field it is no longer possible to determine a normal

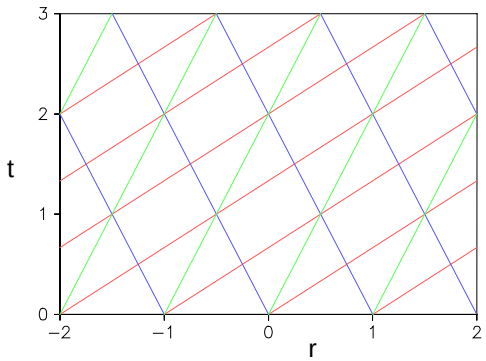

Fig.5 Characteristics in Eulerian frame; advancing, receding, convective (projected)

to the wave fronts and Eqs.(21) and (22) become irrelevant. Inspection of the remaining Eqs.(23) and Eq.(24) shows that in that case the solution of these equations is trivial and can be performed in any convenient coordinate system.

In general the right hand sides of Eqs.(21) and (22) have to be computed numerically. However for cylindrically (n_{dim} = 2) and spherically (n_{dim} = 3) symmetric waves they can be evaluated analytically and then Eqs.(21) and (22) reduce to :

$$\left[\frac{d(p + u)}{dt}\right]_{d\xi/dt = M + 1} = (1 - n_{dim})\frac{u}{\xi - Mt} \qquad (25)$$

and

$$\left[\frac{d(p - u)}{dt}\right]_{d\xi/dt = M - 1} = (1 - n_{dim})\frac{u}{\xi - Mt} \qquad (26)$$

where ξ is a coordinate axis through the center. The radius of curvature of the wave fronts is given by $|\xi - Mt|$.

Non-reflecting boundary conditions

Boundary conditions play a crucial role in CAA and often are more difficult to model than the sound dynamics inside the domain. A comprehensive review on boundary conditions in CAA has been given by Tam[10].

In the present method boundary conditions at domain boundaries are very easily imposed. Acoustically non-reflective boundaries are obtained by just requiring the incoming characteristic variable to be zero.

Note that for acoustic waves incident from outside the domain the wave front orientation is implied in the components of the acoustic velocity v_a, which is also to be prescribed at the exposed boundaries.

As shown by Eqs.(23) and (24), inflow conditions are given by simply prescribing p - ρ and v_h at the inflow boundary. Outflow conditions are automatically satisfied by the solution.

Numerical implementation

Initial conditions

In the present method a problem is basically solved as the evolution in time from a given situation to the situation some time later. If a harmonic problem is to be solved, it has to be treated as a transient problem in which the situation changes from some trivial steady situation to a fully periodic situation. The 'situation' is given as a set of data in a given domain. For the present method the initial data have to be given in the

form of the characteristic variables, see Eqs.(21) through (24). For programming it is convenient if the data points are positioned along isobars (s,q) and normal directions (r). Figure 6 gives an example of a (part of a) circular system that could be the result of a cylindrical or spherical expansion. In any case the unit normal vector on the wave fronts i_r has to be available or computable from the data.

It is not necessary to fill the whole domain with data points at the starting time. This is because the method constructs its own coordinates during the time stepping procedure to follow. In a pure initial value problem the data are given in a certain subdomain (for instance a central pulse) from which the full domain is gradually filled as time proceeds.

A slightly different type of problem is to be solved when the medium within the domain is at rest in the beginning and perturbations enter the domain from outside. Then, there are no data points at all inside the domain at the start but the domain is gradually filled from the exposed sides. Again, it is convenient if the data points of the incident field are wave front oriented.

Time stepping

Before a time step can actually be taken, the possible change of the wave front orientation has to be evaluated and the unit propagation vector i_r has to be updated. To this end, a second order accurate central difference pressure gradient is taken for all data points.

Next, the divergence of the updated vector field i_r has to be established in all data points. Instead of trying to compute the divergence from its definition by numerical differentiation we will use Gauss' divergence theorem:

$$\int_V \nabla\bullet A\,dv = \oint_S n\bullet A\,ds \qquad (27)$$

Here A is a vector field, V a volume, S the enclosing surface and n the outward unit normal vector. Applying the 2D version of Eq. (27) to vector field i_r and a small volume enclosing the point (i,j) considered we obtain:

$$\int_V \nabla\bullet i_r\,dv = \Delta s_{i+1} - \Delta s_{i-1} \qquad (28)$$

where Δs is the arc length between characteristics j+1 and j-1. Since the volume is approximated by $\left(\Delta s_{i+1} - \Delta s_{i-1}\right)R_i$, with R_i the local radius of curvature of the isobar, the average value of the divergence of i_r is given by

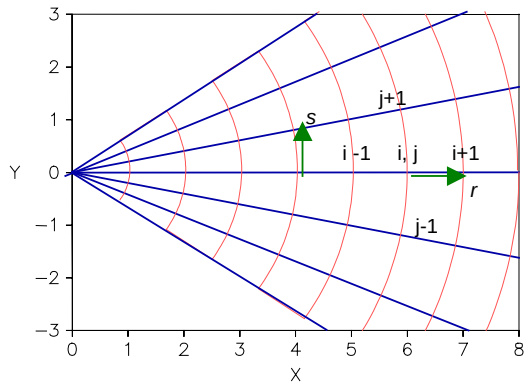

Fig.6 Isobars (——) and projected characteristics (——) for curvilinear wave fronts

$$\overline{\nabla\bullet i_r} \approx 1/R_i \qquad (29)$$

which is exact for cylindrically symmetric cases as shown by the result found earlier in Eqs.(25) and (26). However, in general the radius of curvature of the isobars is not known in advance and has to be found numerically. Therefore in the implementation of the method R_i is computed from the intersection of neighboring vectors i_r.

The actual time integration of Eqs.(21) through (24) is performed by the classical fourth order Runge-Kutta method[7] . As shown in Fig.5, the initial spacing in r determines the time step, which necessarily results in a unit CFL number in r-direction. For convenience only uniform spacing of isobars is considered in this paper.

Renumbering of characteristics

From Fig.5 it is quite clear that after each time step the advancing characteristic RR (Right running) has moved a corresponding step forward in r and the receding characteristic LR (Left running) a step backward. To reallocate the characteristic variables to the same spatial coordinates, a renumbering is necessary after each time step as follows:

$$\begin{aligned} RR_i &= RR_{i-1}, \qquad LR_i = LR_{i+1} \\ x_i &= x_{i-1} \\ y_i &= y_{i-1} \end{aligned} \qquad (30)$$

Note that for every characteristic direction j two data points travel out of the domain in each time step. This is essentially the radiation from the domain into the outside world. To keep the number of data points constant, at the same time a new advancing characteristic RR_{imin} is added at the lower r-boundary of the domain and a receding characteristic LR_{imax} at the upper r-boundary. The

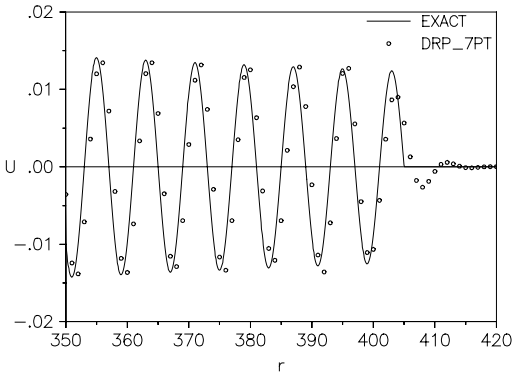

Fig.7 Spherical waves at $t = 400$, $\omega = \pi/4$, Tam & Webb DRP scheme

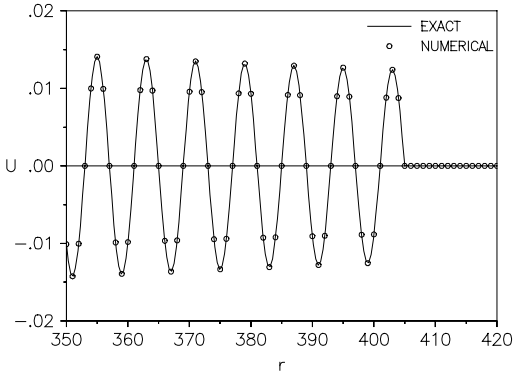

Fig.8 Spherical waves at $t = 400$, $\omega = \pi/4$, present method

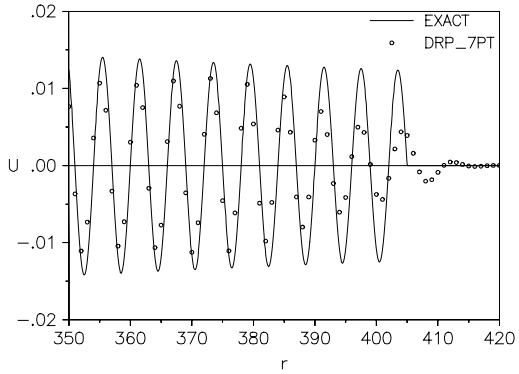

Fig. 9 Spherical waves at $t = 400$, $\omega = \pi/3$, Tam & Webb DRP scheme

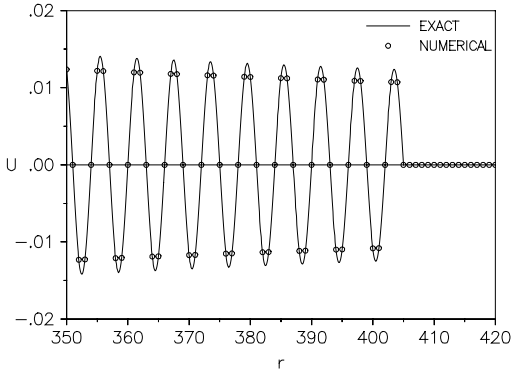

Fig. 10 Spherical waves at $t = 400$, $\omega = \pi/3$, present method

corresponding values of the characteristic variables follow from the boundary conditions.
Finally, the transformation to fixed frame of reference is established by shifting the data points over the distance covered by convection. Similarly to the above, new data points are introduced at the upstream boundary whenever data points are convected out of the domain at the downstream boundary.

Quasi-1D problems in 2D and 3D

Vibrating sphere

As an example of the potential of the present method we give here the solution of the second Cat.1 benchmark problem of the first CAA Workshop[8]. This is a problem in which the sound field of a vibrating sphere is simulated. The radius of the sphere is 5 units and the vibration is switched on at t = 0. For comparison with the state of the art in CAA, Fig.7 gives the results of the Tam & Webb Dispersion Relation Preserving (DRP) scheme for t = 400. The frequency has been chosen such that there are 8 grid points per wavelength. Obviously, the results are quite good at some wavelengths behind the advancing front. However, in the vicinity of the outer front discrepancies appear. In Fig.8 the results of the present characteristics method are given. Clearly, there is no visible difference with the exact solution.
As shown in Fig.9, the results of the DRP scheme degrade considerably when the frequency is increased such that there are 6 points per wavelength left. In contrast to this, the results of the present method shown in Fig.10 still coincide perfectly with the exact solution. Indeed, the method is insensitive to the number of points per wavelength.

Gaussian pulse in 2D

The Category 3 benchmark problem of the first CAA workshop[8] has become a very popular test case. Basically it is the two-dimensional, symmetric variant of the Gaussian pulse in one dimension, discussed earlier. Besides a Gaussian pulse in the pressure, the full benchmark problem also contains perturbations in density and velocity corresponding to a vortex. The analytical solution can be found in references 1 or 8. Here we will use only the pressure pulse to check the present method. One of the interesting aspects of this initial value problem is that both inward and out-

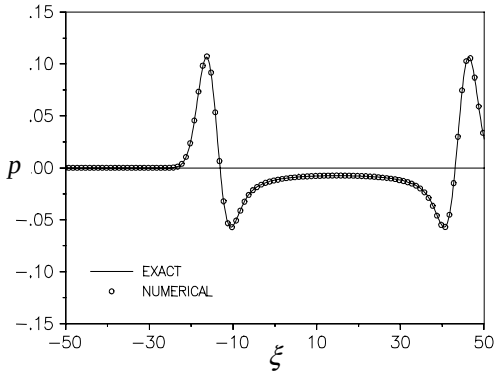

Fig. 11 Cylindrical Gaussian pulse $t = 30$, $M = 0.5$

ward running waves occur. Because u = 0 at t = 0, they start with equal strength, see Eqs.(25) and (26).

Figure 11 shows the results of the method after 30 time units from the start in the center. Due to a mean flow Mach number of 0.5 the pulse is convected downstream whilst expanding. Again, there is no visible difference between the numerical and the exact results. It must be noted that the DRP-scheme is also quite capable to produce very good results[1,8] for this smooth problem. However, the present method typically is a factor of 30 faster than the DRP-method for this problem. There are two obvious reasons for this. First, the unit time step is much larger than the maximum time step for stability in the DRP-scheme ($\Delta t \approx 0.2$). Secondly, the spatial stencil used to compute the pressure gradient is much more compact (only four neighboring points) than in the DRP-scheme.

Gaussian pulse in 3D

Another test case is the expansion of a spherical Gaussian pulse. The general exact solution for any spherically symmetric pressure pulse is given by

$$p(\xi,t) = \frac{\xi-(1+M)t}{2(\xi-Mt)}\,p[\xi-(1+M)t,0] + \frac{\xi+(1-M)t}{2(\xi-Mt)}\,p[\xi+(1-M)t,0] \qquad (31)$$

Starting with the same pulse as in the 2D example, we solve Eqs.(25) and (26) numerically .The solution for M=0.5 after 30 time units is presented in Fig.12. Compared to the cylindrical pulse in Fig.11 the amplitude has decreased much faster and also the inner region has virtually returned to undisturbed conditions.

Triangular pulse in 3D

A more challenging problem is the expansion in three dimensions of a triangular pressure pulse. Let the pressure at t = 0 be given by:

$$\begin{aligned} p &= 1-|\xi|/10, && |\xi| \le 10 \\ p &= 0, && |\xi| > 10 \end{aligned} \qquad (32)$$

Then the exact solution is readily obtained from Eq.(31). As shown in Fig.13, the method of characteristics produces a result of similar quality as for the smooth pulse in Fig.12. Note that the original discontinuity in the pressure derivative in x = 0 completely disappears during the expansion.

Some propagation problems in 2D

All problems in the previous section were symmetric and could be solved from Eqs.(25) and (26). These equations have a simple right hand side, which can be readily computed. Usually, problems do not exhibit symmetry and we will have to solve the more general Eqs.(21) through.(24). As discussed in a previous section the right hand side in Eqs. (21) and (22) involves serious computation.

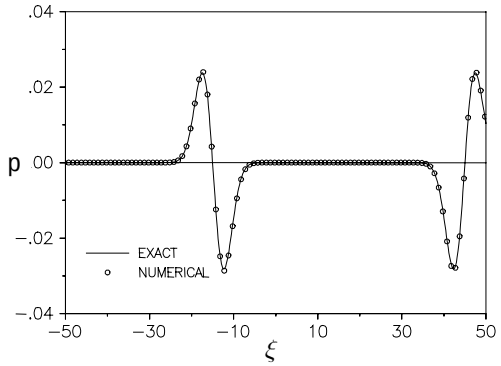

Fig. 12 Spherical Gaussian pulse, $t = 30$, $M = 0.5$

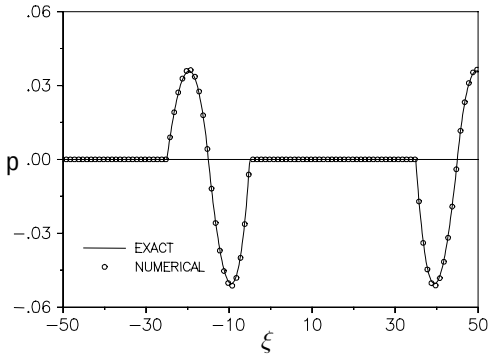

Fig.13 Spherical wave from triangular pulse, $t = 30$, $M = 0.5$

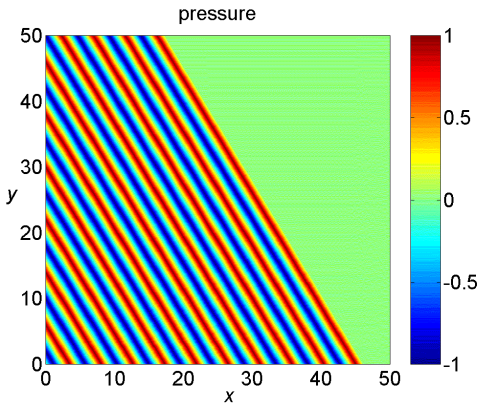

Fig.14 Oblique plane wave, incident field prescribed at left and lower boundaries, t =40, M = 0

Oblique plane waves in 2D

A well-known situation is a domain in which we have to compute the sound field for given boundary conditions. One of the simplest problems possible is a rectangular domain exposed to a system of plane waves propagating through the domain. The present method is tested on this problem and the results are shown in Fig.14. A system of plane waves propagating at an angle of 30 degrees with the horizontal axis enters the lower left corner of the domain at t = 0. As shown in Fig.14, at t = 40 the left and lower boundaries are fully exposed to the wave system. At the right and upper faces nonreflecting boundary conditions are imposed.
Figure 15 presents the pressure along the propagation direction passing through the origin. It is clear that there is a perfect agreement with the exact solution. This problem may look an oversimplified test case, but most numerical schemes have great difficulty to compute this transient problem for a comparable grid density.

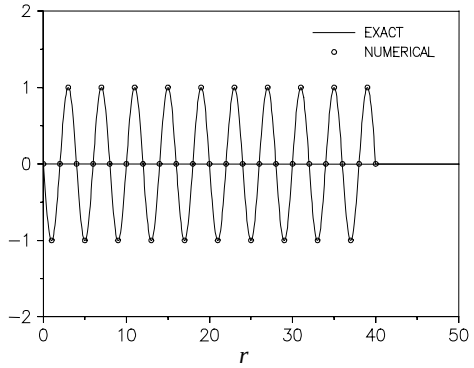

Fig. 15 Pressure along normal to oblique wave fronts in Fig.12, four points per wavelength

Cylindrical Gaussian pulse

A similar test case can be constructed for a cylindrical Gaussian pulse, as discussed before, but now propagating through a rectangular domain whilst expanding. As shown in Fig.16, we consider a domain with a lower left corner (50,50). The pulse has its center at the origin outside the domain and the time starts at t = 0. The exact characteristic variables along the exposed faces are computed every time level (dt = 1). The field propagates freely into the domain and computes its own propagation vector at every time level.
From Figs.16 (t = 100) and 17 (t = 130) it appears that the pulse indeed expands without any reflection from the boundaries. Also the circular symmetry is impeccably maintained.
The pressure field along the diagonal given in Fig.18 confirms the very good agreement with the exact solution.

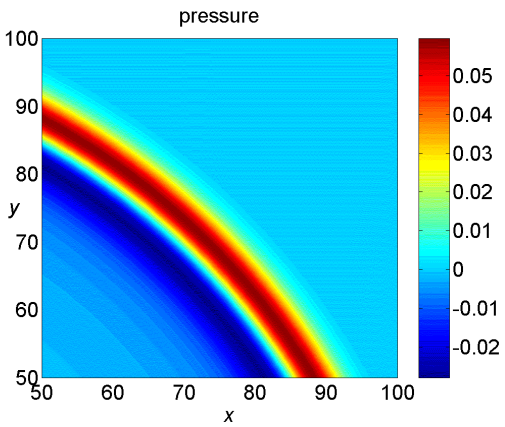

Fig. 16 Gaussian pulse in 2D, t = 100, M = 0, incident field prescribed at left and lower boundaries

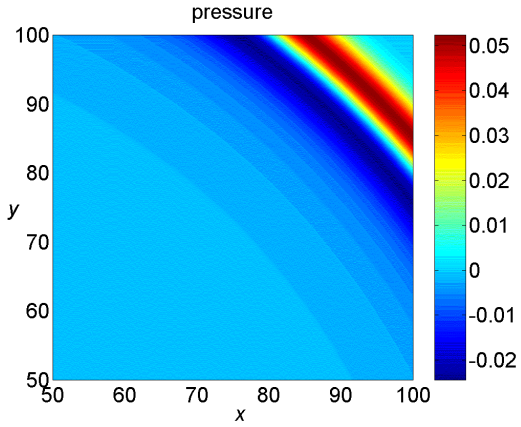

Fig.17 Gaussian pulse in 2D, t = 130, M = 0, incident field prescribed at left and lower boundaries

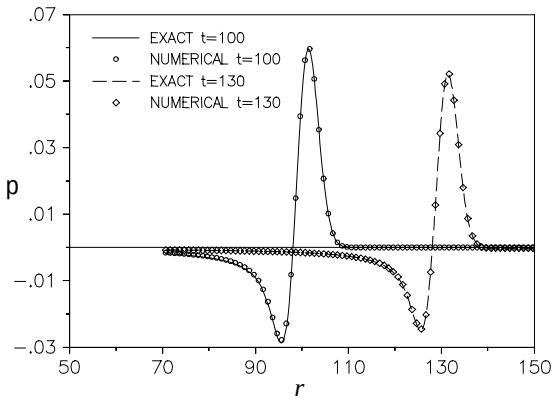

Fig. 18 Pressure along the diagonal in Figs.14 and 15

Acknowledgement

The author wishes to thank his colleague Dr. Ronald Nijboer for many stimulating and helpful discussions. His comments on the first draft of the manuscript led to significant improvements in the present paper.

Concluding remarks

In this paper the method of characteristics is used to compute sound propagation and radiation numerically. Unlike traditional CAA schemes the present method is not based on a fixed grid. Instead the solution is marched in time by following the propagation vectors, i.e. the characteristics. In this respect the method has some similarity with classical ray acoustics. However, the present method is more general and does not require the high frequency assumption.

As shown by two- and three-dimensional benchmark examples, the total absence of numerical dispersion and dissipation leads to very accurate numerical results. The interesting point is that this property also holds for waves of highly irregular shape, including discontinuities.

Exact non-reflecting boundary conditions are easily implemented in a most natural way. This feature alone would already justify further research on the application of the method in more complex problems.

Computationally, the method is very efficient: typically a factor of 30 faster than the DRP-method in the 2D Gaussian pulse benchmark[8].

At the same time it is fair to say that still considerable difficulties have to be surmounted before the method will be applicable to more complex problems. These problems may concern a non-uniform background flow, reflection on hard obstacles, diffraction effects and nonlinearity.

Nevertheless it may be concluded that the method of characteristics has properties that make them very attractive for application in computational aeroacoustics. Its most promising features are the insensitivity to the wave shape, the absence of dissipation and dispersion errors, and the implementation of non-reflecting boundary conditions.

References

[1]Tam, C.K.W., Webb, J.C., "Dispersion-Relation-Preserving Finite Difference Schemes for Computational Acoustics", Journal of Computational Physics, Vol.107, Aug. 1993, pp. 262-281.

[2]Tam, C.K.W., "Computational Aeroacoustics: Issues and Methods", AIAA Journal, Vol. 33, No.10, Oct. 1995, pp. 1788-1796.

[3]Lele, S.K, "Computational Aeroacoustics: A Review", AIAA Paper 97-0018, Jan. 1997

[4]Colonius, T., "Lectures on Computational Aeroacoustics", VKI Lecture series 1997-07: Aeroacoustics and Active Noise Control, Sept. 1997

[5]Pierce, A.D., ACOUSTICS-An Introduction to its Physical Principles and Applications, McGraw Hill, New York, 1981

[6]Toro, E.F., Riemann Solvers and Numerical Methods for Fluid Dynamics, 2nd edition, Springer, Berlin 1999

[7]Press, W.H., Flannery, B.P., Teukolsky, S.A., Vetterling, W.T., Numerical Recipes, Cambridge University Press, 1989

[8]Hardin, J.C. et al., "ICASE/LaRC Workshop Benchmark Problems in Computational Aeroacoustics (CAA)", NASA Conference Publication 3300, May 1995.

[9]Margolin, L., Introduction to "Arbitrary Lagrangian-Eulerian Computing Method for All Flow Speeds", J. Comp. Phys., 135 (1997), pp. 198-202.

[10]Tam, C.K.W., "Advances in Numerical Boundary Conditions for Computational Aeroacoustics", Journal of Computational Acoustics, Vol.6, No.4, 1998, pp. 377-402